



**NO MLT comparison
of ACE-FTS, MIPAS,
SCIAMACHY, and
SMR**

S. Bender et al.

This discussion paper is/has been under review for the journal Atmospheric Measurement Techniques (AMT). Please refer to the corresponding final paper in AMT if available.

Comparison of nitric oxide measurements in the mesosphere and lower thermosphere from ACE-FTS, MIPAS, SCIAMACHY, and SMR

S. Bender¹, M. Sinnhuber¹, T. von Clarmann¹, G. Stiller¹, B. Funke²,
M. López-Puertas², J. Urban^{3,†}, K. Pérot³, K. A. Walker⁴, and J. P. Burrows⁵

¹Institute for Meteorology and Climate Research, Karlsruhe Institute of Technology, Karlsruhe, Germany

²Instituto de Astrofísica de Andalucía, CSIC, Granada, Spain

³Department of Earth and Space Sciences, Chalmers University of Technology, Gothenburg, Sweden

⁴Department of Physics, University of Toronto, Toronto, Canada

⁵Institute of Environmental Physics, University of Bremen, Bremen, Germany

[†]deceased, 14 August 2014

Title Page	
Abstract	Introduction
Conclusions	References
Tables	Figures
◀	▶
◀	▶
Back	Close
Full Screen / Esc	
Printer-friendly Version	
Interactive Discussion	



Received: 8 October 2014 – Accepted: 23 November 2014 – Published: 18 December 2014

Correspondence to: S. Bender (stefan.bender@kit.edu)

Published by Copernicus Publications on behalf of the European Geosciences Union.

AMTD

7, 12735–12794, 2014

NO MLT comparison of ACE-FTS, MIPAS, SCIAMACHY, and SMR

S. Bender et al.

Title Page

Abstract

Introduction

Conclusions

References

Tables

Figures



Back

Close

Full Screen / Esc

Printer-friendly Version

Interactive Discussion



Abstract

We compare the nitric oxide measurements in the mesosphere and lower thermo-
sphere (60 to 150 km) from four instruments: ACE-FTS, MIPAS, SCIAMACHY, and
SMR. We use the daily zonal mean data in that altitude range for the years 2004–2010
(ACE-FTS), 2005–2012 (MIPAS), 2008–2012 (SCIAMACHY), and 2003–2012 (SMR).

We first compare the data qualitatively with respect to the morphology, focussing on
the major features, and then compare the time series directly and quantitatively. In three
geographical regions, we compare the vertical density profiles on coincident measure-
ment days. Since none of the instruments delivers continuous daily measurements in
this altitude region, we carried out a multi-linear regression analysis. This regression
analysis considers annual and semi-annual variability in form of harmonic terms and
inter-annual variability by responding linearly to the solar Lyman- α radiation index and
the geomagnetic Kp index. This analysis helps to find similarities and differences in the
individual data sets with respect to the inter-annual variations caused by geomagnetic
and solar variability.

We find that the data sets are consistent and that they only disagree on minor as-
pects. SMR and ACE-FTS deliver the longest time series in the mesosphere and they
both agree remarkably well. The shorter time series from MIPAS and SCIAMACHY
also agree with them where they overlap. The data agree within ten to twenty percent
when the number densities are large, but they can differ by 50 to 100 % in some cases.

1 Introduction

Climate models aim to predict the trend of Earth's climate considering the composition
of the atmosphere. This composition is influenced by a number of factors, including
anthropogenic emissions and solar variability. To disentangle these effects, the evalu-
ation of the solar influence is important. Solar particles and soft solar X-rays produce
nitric oxide (NO) in the mesosphere and lower thermosphere (MLT, 50–150 km) (Barth

AMTD

7, 12735–12794, 2014

NO MLT comparison of ACE-FTS, MIPAS, SCIAMACHY, and SMR

S. Bender et al.

Title Page

Abstract

Introduction

Conclusions

References

Tables

Figures

◀

▶

◀

▶

Back

Close

Full Screen / Esc

Printer-friendly Version

Interactive Discussion



et al., 2003). Thus, the NO content in this atmospheric region indicates how much solar activity impacts the atmospheric composition and how important solar variability is in climate models.

To relate atmospheric composition changes to solar activity, global NO measurements over long time periods deliver important information. This data is provided by satellite instruments using different measurement methods. The consistency of these measurements is crucial for using the results for further work, for example to validate climate models and to find climate relevant forcing parameters. We compare the daily zonal mean NO number densities from four space-borne instruments: the Michelson Interferometer for Passive Atmospheric Sounding (MIPAS, infrared limb emission) and the SCanning Imaging Absorption spectroMeter for Atmospheric CHartographY (SCIAMACHY, UV-vis-NIR limb and nadir emission) on Envisat, the Sub-Millimetre Radiometer (SMR, sub-mm limb emission) on the Odin satellite, and the Atmospheric Chemistry Experiment–Fourier Transform Spectrometer (ACE-FTS, infrared solar occultation) on SCISAT. The aim of this comparison is to answer the question whether zonal mean data sets from different instruments consistently constrain the nitric oxide in the MLT.

The instruments are introduced in Sect. 2. In a first comparison step, we compare zonal daily mean distributions in an altitude range from 75 to 115 km (Sect. 3). In that section we analyse the time–latitude morphology of the NO number densities at different times of solar activity, from low (2008/09) to moderate (2010/11). In Sect. 4 we directly compare the time series of NO number densities at selected geographic locations. This more quantitative comparison emphasizes differences which cannot be detected in the morphological comparison. We further compare daily mean vertical profiles in order to detect differences that may result from the different retrieval strategies (Sect. 5). In Sect. 6, we extend the comparison towards derived diagnostic quantities of particular scientific interest, for example regression coefficients for the contribution of Lyman- α and the geomagnetic Kp index. In the Conclusions (Sect. 7) we evaluate the consistency of the analysed data sets.

**NO MLT comparison
of ACE-FTS, MIPAS,
SCIAMACHY, and
SMR**

S. Bender et al.

Title Page

Abstract

Introduction

Conclusions

References

Tables

Figures



Back

Close

Full Screen / Esc

Printer-friendly Version

Interactive Discussion



2 Instruments

2.1 Envisat/MIPAS

Two of the instruments considered here, MIPAS and SCIAMACHY, are on board the now defunct European research satellite Envisat. This satellite has been orbiting on a sun-synchronous orbit at 800 km and at equator crossing times 10:00/22:00 since 2002. Communication to the satellite was lost in April 2012, which is therefore the latest date for which MIPAS and SCIAMACHY data are available.

The Michelson Interferometer for Passive Atmospheric Sounding (MIPAS) is an infrared Fourier transform spectrometer. It has a spectral range from 4.15 to 14.6 μm (685–2410 cm^{-1}), and the spectral resolution was 0.0625 cm^{-1} during the relevant time period. The instrument has an instantaneous field of view of 3 km in the vertical and 30 km in the horizontal direction.

MIPAS measured atmospheric emissions in a limb observation geometry (Fischer et al. 2008). The instrument provided two special observation modes dedicated to the middle atmosphere (MA, 18–102 km) and upper atmosphere (UA, 42–172 km) (Raspollini et al., 2013). After a test phase of twelve measurement days from January 2005 to October 2007, about one day every three months, the measurements using these modes were scheduled regularly on two days every 10 days of nominal mode measurements (7–72 km) since November 2007. In this study, we use only the day side half-orbit (downleg, am) MIPAS-UA measurements, which amount to 199 measurement days with about 500 scans per day from 21 January 2005 until 30 March 2012.

The NO data used here were produced using the MIPAS data processor developed at the Institute of Meteorology and Climate Research (IMK) in cooperation with the Instituto de Astrofísica de Andalucía (IAA) (von Clarmann et al., 2003). The retrieval is based on constrained multi-parameter non-linear least squares fitting of observed to calculated radiance spectra. The retrieval processor was extended to apply to non-local thermodynamic equilibrium (Non-LTE) emissions (Funke et al., 2001), which is partic-

NO MLT comparison of ACE-FTS, MIPAS, SCIAMACHY, and SMR

S. Bender et al.

Title Page

Abstract

Introduction

Conclusions

References

Tables

Figures



Back

Close

Full Screen / Esc

Printer-friendly Version

Interactive Discussion



ularly important for NO retrievals. The vibrational, rotational, and spin level populations under Non-LTE were modelled by the Generic RAdiative traNSfer AnD non-LTE population Algorithm (GRANADA) (Funke et al., 2012) during each iteration of the retrieval.

NO in the altitude region of interest (70–120 km) is derived from the fundamental NO band emission at 5.3 μm . The retrieval of NO in the middle atmosphere (up to ~ 100 km) is described in detail in Funke et al. (2005). The NO data used here (Versions V5r_NO_520 (MA) and V5r_NO_620 (UA)) were measured from January 2005 to April 2012, when MIPAS used a slightly degraded spectral resolution. The data version described in Funke et al. (2005) has been substantially improved as summarised in Funke et al. (2014), and the present version includes these improvements.

The single profile vertical resolution of NO in the 70–100 km region is 15–20 km and the single profile precision ranges from $\sim 50\%$ at 70 km to $\sim 30\%$ at 100 km. In general, MIPAS has low sensitivity to NO outside of the polar winter region (latitudes greater than 50°) at altitudes of 70–90 km. Systematic errors in the NO VMR in this region amount to around 10%.

The retrieval of NO in the upper atmosphere (100–170 km) is described in detail in Bermejo-Pantaleón et al. (2011). Temperature and nitric oxide mixing ratio profiles are retrieved jointly in this region. The typical single measurement precision of NO in this region is 10–30% for high geomagnetic activity, increasing to 20–50% for low geomagnetic activity. The vertical resolution is 5–10 km for high geomagnetic activity and degrades to 10–20 km for low geomagnetic activity. For extra-polar and low geomagnetic activity, a potential systematic bias in the nighttime NO version V4O_NO_611 profiles was identified (Bermejo-Pantaleón et al., 2011). This bias is caused by smoothing errors and was corrected in the current version V5r_NO_620 by using an appropriate a priori NO profile for nighttime conditions. The retrieved NO abundances in the thermosphere depend strongly on the assumed atomic oxygen above 120 km, which was taken from the NRL-MSISE-00 model. Other systematic errors as the uncertainties in the atomic nitrogen and the propensity for spin-conserving collisions, which largely

**NO MLT comparison
of ACE-FTS, MIPAS,
SCIAMACHY, and
SMR**

S. Bender et al.

Title Page

Abstract

Introduction

Conclusions

References

Tables

Figures



Back

Close

Full Screen / Esc

Printer-friendly Version

Interactive Discussion



use". The MIPAS and SCIAMACHY data are filtered based on the average diagonal element of the averaging kernel matrix. The thresholds are 0.003 for MIPAS and 0.01 for SCIAMACHY. The SMR data are filtered using the measurement response which is the sum of the rows of the averaging kernel matrix. All zonal mean boxes with a mean measurement response below 0.75 were not considered.

3 Zonal mean data

Figures 1 and 2 show the zonal mean data at altitudes of 85 and 105 km from all instruments: ACE-FTS, MIPAS, SCIAMACHY, and SMR. The zonal mean data at additional altitudes from 75 to 115 km are shown in Figs. A1 to A5.

These figures give an overview of the available data set. ACE-FTS, as a solar occultation instrument, has only limited geographical coverage. MIPAS and SMR have limited sensitivity at altitudes below 85 km, in particular at middle and low latitudes. Additionally, MIPAS data from 75 to 100 km is at present only available since July 2008. The SCIAMACHY data are restricted to daytime measurements which adversely affects the number of measurements, in particular at high latitudes in the polar winter. SMR data are relatively sparse before 2007 when the Odin astronomy mission ended and more measurement days were dedicated to NO observations since then.

The zonal mean data of all four instruments are consistent with respect to the annual variation of the NO density in the MLT region. Throughout the latitude range, the number densities are low at times of low solar activity, 2008 and 2009, and increase with growing solar activity, 2010 and 2011. The NO density increases most in the polar regions and at higher altitudes. Between 95 and 115 km, the density increases also at lower latitudes, in particular after 2011.

NO MLT comparison of ACE-FTS, MIPAS, SCIAMACHY, and SMR

S. Bender et al.

Title Page

Abstract

Introduction

Conclusions

References

Tables

Figures



Back

Close

Full Screen / Esc

Printer-friendly Version

Interactive Discussion



4 Time series

To put the comparisons from Sect. 3 onto more quantitative grounds, we directly compare the NO density time series in four different 5° latitude bins and at altitudes from 75 to 115 km. These bins are located at high northern (67.5° N) and high southern latitudes (67.5° S), at middle latitudes (32.5° S), and at low latitudes (2.5° N) near the equator.

4.1 Northern Hemisphere

We first compare the values in the Northern Hemisphere at 67.5° N. Figure 3 shows the time series at two example altitudes, 85 km (upper mesosphere) and 105 km (lower thermosphere). Figure B1 shows the time series at more altitudes from 75 to 115 km.

The results are consistent throughout the altitude range, the largest values are observed between 95 and 105 km and smaller values below and above these altitudes. Only SMR and ACE-FTS provide data below 100 km for the years 2004 to 2008. Above 100 km, MIPAS contributes some data points from 2005 onwards, and SCIAMACHY data are available only from mid-2008.

ACE-FTS, SMR, and MIPAS show that the NO number density is correlated with solar activity. From 2004 to 2007, a period of moderate solar activity, the number densities were generally larger than in 2008/09, when solar activity was low. The NO density increases then again after 2009 with the onset of the next solar cycle. This correlation is visible at all altitudes and it is particularly strong in the main production region from 95 to 105 km. Unfortunately, the SCIAMACHY data set is too short to show the same correlation. The SCIAMACHY number densities are always on the low side compared to the other instruments. This is less pronounced at 75 km but is clearly visible at altitudes of 85 km and above.

In addition to the overall correlation of the NO densities with the long-term solar activity, the seasonal cycle is clearly visible in the data from all instruments. This annual variation is more pronounced at 85 km, but it is also visible at 105 km.

NO MLT comparison of ACE-FTS, MIPAS, SCIAMACHY, and SMR

S. Bender et al.

Title Page

Abstract

Introduction

Conclusions

References

Tables

Figures



Back

Close

Full Screen / Esc

Printer-friendly Version

Interactive Discussion



southern polar region (90–50° S), at middle and low latitudes outside the polar regions (50° S–50° N), and in the northern polar region (50–90° N).

MIPAS and SCIAMACHY share the same satellite and therefore they performed the most congruent measurements. In addition, their limb scans were scheduled to measure the mesosphere and lower thermosphere during the same orbits once a month. Therefore, we get the best statistics from this pair of instruments.

SCIAMACHY has fewer coincident days with SMR than with MIPAS. We also have to consider the different local times of the measurements, which are 10:00 for SCIAMACHY and between 06:00 and 07:00 for SMR (at the equator). This timing of the SMR measurements makes them susceptible to the NO diurnal cycle and may lead to systematic differences in the measured number densities, in particular in the lower mesosphere. The coincidences with ACE-FTS amount to only about ten to twenty usable profiles. Since ACE-FTS measures at sunrise and sunset primarily at higher latitudes, the NO diurnal cycle also affects the retrieved number densities.

The patterns of the MIPAS to SCIAMACHY differences in Fig. 7 are similar in all three regions. The magnitude of the difference varies slightly with the region, it is smallest at middle and low latitudes and at high northern latitudes. Between 120 and 140 km, the MIPAS and SCIAMACHY number densities agree well in all three regions, the SCIAMACHY NO densities differ only slightly from the MIPAS measured densities. In the main production region from 100 to 120 km, SCIAMACHY significantly underestimates the NO number densities compared to MIPAS measurements by about 50 % at high southern latitudes and by about 40 % at middle and low latitudes and at high northern latitudes. Between 70 and 95 km in the northern polar region, the SCIAMACHY NO number densities are larger than the measurements from ACE-FTS and MIPAS. The SCIAMACHY data are consistent with the other instruments at these altitudes in the southern polar region and at middle and low latitudes.

SCIAMACHY consistently measures lower number densities than SMR by 10 to 20 %. The data agree from 80 to 100 km in the northern polar region. At middle and low latitudes, the SCIAMACHY and SMR densities agree at 95 and at 110 km.

**NO MLT comparison
of ACE-FTS, MIPAS,
SCIAMACHY, and
SMR**

S. Bender et al.

Title Page

Abstract

Introduction

Conclusions

References

Tables

Figures



Back

Close

Full Screen / Esc

Printer-friendly Version

Interactive Discussion



The SCIAMACHY data agree well with the ACE-FTS data in the Northern Hemisphere. In the Southern Hemisphere, the SCIAMACHY measurements are smaller than the ACE-FTS number densities between 90 and 105 km. Both number densities are consistent below 90 km considering the statistical error. At middle and low latitudes both instruments agree within the large error range.

5.2 Other instruments

Figure 8 shows the median of the relative differences comparing MIPAS data to the other instruments. In all three regions, MIPAS measures the largest NO number densities between 100 and 120 km, between 80 and 120 % larger than measured by the other instruments. As seen in the previous section, MIPAS and SCIAMACHY data agree in all three latitude regions at altitudes between 120 and 140 km. In the northern polar region and at middle and low latitudes, both results agree also between 80 and 95 km. In the southern polar region, the MIPAS measurements are about 50 to 100 % larger than the SCIAMACHY measurements from 70 to 95 km.

Between 80 and 100 km in the southern polar region, the MIPAS and the ACE-FTS data agree well. Below 80 and above 100 km in this region, the MIPAS number densities are larger by 50 to 100 %. At middle and low latitudes MIPAS and ACE-FTS have only a few coincident measurement days and even less comparable data points when considering the instruments' sensitivity. In the upper usable altitude region, between 95 and 105 km, MIPAS and ACE-FTS are consistent. In the lower altitude region from 65 to 70 km, MIPAS number densities are larger by 50 to 80 %. In the northern polar region, the MIPAS number densities are also larger than the ACE-FTS measurements in the same altitude region. They are smaller than the ACE-FTS number densities between 85 and 100 km.

Compared to SMR, the MIPAS NO number densities are significantly smaller in the southern polar region from 80 to 100 km by about 40 to 50 %. In the northern polar region from 80 to 100 km, the MIPAS number densities are about 30 to 50 % smaller than the SMR data. Above and below, MIPAS and SMR agree within the statistical

NO MLT comparison of ACE-FTS, MIPAS, SCIAMACHY, and SMR

S. Bender et al.

Title Page

Abstract

Introduction

Conclusions

References

Tables

Figures



Back

Close

Full Screen / Esc

Printer-friendly Version

Interactive Discussion



error. Both number densities agree well at middle and low latitudes between 90 and 100 km.

Figure 9 shows the median of the relative profile differences comparing the SMR data to the other measurements. In all three regions, the SMR number densities are consistently larger than the SCIAMACHY data above 100 km. We observe the largest differences in the southern polar region, up to 80 %. However, both number densities agree in the northern polar region from 80 to 100 km. At middle and low latitudes, the difference between SMR and SCIAMACHY vary between 10 and 40 %, reaching larger but insignificant values between 85 and 90 km.

Compared to MIPAS, the SMR number densities are significantly smaller in all three regions from 100 to 120 km by 20 to 50 %. From 85 to 100 km, the SMR number densities are consistently larger than the MIPAS data, in the southern polar region between 50 and 80 %, and in the northern polar region up to 120 % but with a large uncertainty. At middle and low latitudes, both measurements are consistent between 90 and 105 km.

Compared to ACE-FTS, the SMR number densities are substantially larger at high southern latitudes above 100 km, differing by 100 % at 105 km. ACE-FTS and SMR data agree well between 80 and 100 km. Below 80 km in that region, the SMR number densities differ from the ACE-FTS results between 50 and 80 % but with a large statistical uncertainty. Both NO number densities are comparable at middle and low latitudes over the whole altitude range considering the statistics. The differences in the northern polar region behave similarly to the results at high southern latitudes, the maximum deviation is 150 % at 105 km. Here, both data sets agree well between 90 and 100 km. The SMR number densities are up to 60 % larger than the ACE-FTS data below 90 km in that region.

Figure 10 shows the median of the relative profile differences of the ACE-FTS NO number densities to the other instruments. It summarises the above discussion from ACE-FTS' point of view, showing the best agreement with MIPAS and SMR in the southern polar region from 85 to 100 km, and with SCIAMACHY and SMR in the north-

**NO MLT comparison
of ACE-FTS, MIPAS,
SCIAMACHY, and
SMR**

S. Bender et al.

Title Page

Abstract

Introduction

Conclusions

References

Tables

Figures



Back

Close

Full Screen / Esc

Printer-friendly Version

Interactive Discussion



ern polar region from 80 to 100 km. The ACE-FTS number densities are substantially larger than the SCIAMACHY measurements in the southern polar region between 90 and 105 km. They also differ significantly from the MIPAS data in the northern polar region between 85 and 100 km. At middle and low latitudes, the ACE-FTS measurements are smaller than all other number densities from 70 to 100 km by 40 to 100 %.

6 Multi-linear regression analysis

The direct quantitative comparison of the NO data of the four instruments is difficult for several reasons. Coincident measurements are sparse and the local times of the individual measurements differ substantially between some of the instruments. The solar UV radiation influences the NO density annually because of the different solar inclination, and inter-annually due to its varying intensity during the eleven-year solar cycle. Then, the NO density can vary substantially from day to day depending on particle precipitation rates, for example at times of high geomagnetic activity.

All instruments scanned the MLT region only on particular single days, for example MIPAS every 10 days and SCIAMACHY every 14 days. In addition, the MIPAS and SCIAMACHY data are only available for the later part of the time period. This makes capturing all variations of NO in the upper atmosphere difficult. To overcome these shortcomings, we carry out a multi-linear regression analysis of the zonal mean data.

We construct a simple transfer function for the NO number density n_{NO} for our multi-instrument intercomparison on non-coincident days. This function includes an offset, annual and semi-annual harmonic terms, and accounts for the solar cycle activity proportional to the UV Lyman- α flux. It also includes a term for daily NO variations caused by geomagnetic activity using the Kp index.

NO MLT comparison of ACE-FTS, MIPAS, SCIAMACHY, and SMR

S. Bender et al.

Title Page

Abstract

Introduction

Conclusions

References

Tables

Figures



Back

Close

Full Screen / Esc

Printer-friendly Version

Interactive Discussion



The NO number density n_{NO} at altitude z , latitude ϕ , and time t is described by:

$$n_{\text{NO}}^{\text{model}}(\phi, z, t) = a(\phi, z) + b(\phi, z) \cdot \text{Ly}\alpha(t) + c(\phi, z) \cdot \text{Kp}(t) + \sum_{n=1}^2 [d_n(\phi, z) \cos(n\omega t) + e_n(\phi, z) \sin(n\omega t)] . \quad (1)$$

In the regression model Eq. (1) a is the constant offset, d_1 and e_1 are the annual, and d_2 and e_2 are the semi-annual cycles with $\omega = 2\pi/(365.25 \text{ d})$ and t in days. This approach accounts for both, amplitude and phase of the cycles. The coefficients b and c refer to the solar Lyman- α flux ($\text{Ly}\alpha$) and the geomagnetic Kp index. We also tested other parameter sets, e.g., the solar radio flux f10.7 for the solar cycle variations and Ap as a geomagnetic proxy. We found that they did not improve the fit and that the combination Lyman- α and Kp gave the best fits. The Kp index is taken from the SPIDR database (NGDC and NOAA, 2011) and the Lyman- α index from the LISIRD database (DeLand and Cebula, 2008; DeWolfe et al., 2010; LISIRD Data Systems Group, 2010).

The time series of the measurements, the regression result fitting the data from all instruments simultaneously, and the residuals are shown in Figs. 11 and 12 for 85 and 105 km at 67.5° N. The same data at 67.5° S are shown in Figs. 13 and 14. The regression results without the residuals at more altitudes (75 to 115 km) and at additional latitudes (32.5° S and 2.5° N) are shown in Figs. C1 to C4.

The solid line in these in the upper panels of these figures is the regression fit using the composite data from all instruments simultaneously. The residuals in the lower panels in these figures indicate that the model Eq. (1) captures most but not all variations in the NO data. While at 105 km, the residuals are mostly randomly distributed with some outliers, they show residual patterns at 85 km. Most of the time, the residuals vary around $\pm 1 \times 10^8 \text{ cm}^{-3}$ at lower altitudes, where the number densities take values between 0 and $6 \times 10^8 \text{ cm}^{-3}$. At higher altitudes the residuals vary between -2 and $+2 \times 10^8 \text{ cm}^{-3}$ with the number densities varying between 0 and $8 \times 10^8 \text{ cm}^{-3}$.

NO MLT comparison of ACE-FTS, MIPAS, SCIAMACHY, and SMR

S. Bender et al.

Title Page	
Abstract	Introduction
Conclusions	References
Tables	Figures
◀	▶
◀	▶
Back	Close
Full Screen / Esc	
Printer-friendly Version	
Interactive Discussion	



Figure 15 shows the relative mean residuals (RMR) of the individual measurements to the composite fit. The RMR are defined as

$$\text{RMR} := \frac{\sum_i \left(n_{\text{NO}}^{\text{meas}}(t_i) - n_{\text{NO}}^{\text{model}}(t_i) \right)}{\sum_i n_{\text{NO}}^{\text{model}}(t_i)}, \quad (2)$$

where $n_{\text{NO}}^{\text{meas}}$ and $n_{\text{NO}}^{\text{model}}$ are the measured and modelled NO number densities. Here, modelled data means applying the coefficients from the composite fit to the days t_i of the individual measurements. The marked boxes in Fig. 15 indicate 95 % significance determined by the F test (Brook and Arnold, 1985; Neter et al., 1996). The ACE-FTS number densities are larger than the composite by about 10 to 30 % where the fit is significant. The same is true for the MIPAS data, except between 70 and 105 km at middle to high northern latitudes. There, the MIPAS number densities are smaller by about the same amount. The SCIAMACHY number densities are smaller than the composite fit by about 10 to 30 % above 90 km throughout the latitude range. They are slightly larger below 90 km, and substantially so between 75 and 85 km at 77.5° S. The SMR number densities are larger than the composite fit by about 10 to 20 % almost everywhere, except at the highest altitudes at middle and low latitudes.

We next analyse the coefficients of the individual regressions to compare the instruments' responses to the harmonic cycles and in particular to Lyman- α and Kp changes. Figures 16 and 17 show the cosine coefficients d_1 and d_2 of the annual and semi-annual cycle. Values with a larger than 95 % significance, calculated from t statistics, are marked with crosses. We find that these coefficients have about the same values for all instruments. The MIPAS, SCIAMACHY, and SMR d_1 coefficients agree remarkably well. The SMR coefficients take high values below 80 km, but these values are not significant. The ACE-FTS coefficients, however, differ substantially at latitudes larger than 60°. The d_2 coefficients agree not as strongly, but they are also one order of mag-

NO MLT comparison of ACE-FTS, MIPAS, SCIAMACHY, and SMR

S. Bender et al.

Title Page

Abstract

Introduction

Conclusions

References

Tables

Figures



Back

Close

Full Screen / Esc

Printer-friendly Version

Interactive Discussion



nitude smaller in general. The sine coefficients e_1 and e_2 are not shown, but they agree on a similar level with a slightly smaller magnitude than their cosine counterparts.

Figures 18 and 19 show the coefficients b and c of the Lyman- α UV index and the Kp geomagnetic index. The latitude-altitude patterns of both coefficients are similar for all instruments. The SMR and SCIAMACHY Lyman- α coefficients b are enhanced at all latitudes in a band from 95 to 110 and 115 km. This band of larger values is less pronounced in the ACE-FTS and MIPAS data. The coefficients are also consistently enhanced at polar latitudes from 80 to 100 km in the ACE-FTS, MIPAS, and SMR data. The coefficients derived from SCIAMACHY data are increased only in the northern polar region.

We observe enhanced Kp coefficients c in the main production regions north and south with all instruments. The magnitude of these coefficients is smallest in the SCIAMACHY data because polar night measurements were rare and only performed during a period of low solar activity. ACE-FTS also provides only few data points at the beginning and the end of the polar night, see Figs. 1 and 2. But in contrast to SCIAMACHY, ACE-FTS measured also during a period of higher solar activity which explains the larger Kp coefficients. The patterns, however, are consistent with the data from the other instruments.

7 Conclusions

In this study, we compared the measurements from four instruments, three limb sounders and one solar occultation instrument, using different spectral ranges: infrared, sub-millimetre waves, and ultra-violet. Despite these different methods and accompanying different retrieval strategies, the nitric oxide daily zonal mean densities of all four instruments are consistent during the comparison time period. However, the instruments have different altitude resolutions. But, as single selected profiles show, the structures of the NO density in the MLT region are larger than the instruments' altitude

NO MLT comparison of ACE-FTS, MIPAS, SCIAMACHY, and SMR

S. Bender et al.

Title Page

Abstract

Introduction

Conclusions

References

Tables

Figures



Back

Close

Full Screen / Esc

Printer-friendly Version

Interactive Discussion



NO MLT comparison of ACE-FTS, MIPAS, SCIAMACHY, and SMR

S. Bender et al.

Title Page

Abstract

Introduction

Conclusions

References

Tables

Figures



Back

Close

Full Screen / Esc

Printer-friendly Version

Interactive Discussion



nonlocal thermodynamic equilibrium emissions measured by Michelson Interferometer for Passive Atmospheric Sounding (MIPAS) on Envisat, *J. Geophys. Res.*, 110, D09302, doi:10.1029/2004JD005225, 2005. 12740, 12743

Funke, B., López-Puertas, M., García-Comas, M., Kaufmann, M., Höpfner, M., and Stiller, G.: GRANADA: A Generic RAdiative traNsfer AnD non-LTE population algorithm, *J. Quant. Spectrosc. Ra.*, 113, 1771–1817, doi:10.1016/j.jqsrt.2012.05.001, 2012. 12740

Funke, B., López-Puertas, M., Stiller, G. P., and von Clarmann, T.: Mesospheric and stratospheric NO_y produced by energetic particle precipitation during 2002–2012, *J. Geophys. Res.*, 119, 4429–4446, doi:10.1002/2013JD021404, 2014. 12740

Kerzenmacher, T., Wolff, M. A., Strong, K., Dupuy, E., Walker, K. A., Amekudzi, L. K., Batchelor, R. L., Bernath, P. F., Berthet, G., Blumenstock, T., Boone, C. D., Bramstedt, K., Brogniez, C., Brohede, S., Burrows, J. P., Catoire, V., Dodion, J., Drummond, J. R., Dufour, D. G., Funke, B., Fussen, D., Goutail, F., Griffith, D. W. T., Haley, C. S., Hendrick, F., Höpfner, M., Huret, N., Jones, N., Kar, J., Kramer, I., Llewellyn, E. J., López-Puertas, M., Manney, G., McElroy, C. T., McLinden, C. A., Melo, S., Mikuteit, S., Murtagh, D., Nichitiu, F., Notholt, J., Nowlan, C., Piccolo, C., Pommereau, J.-P., Randall, C., Raspollini, P., Ridolfi, M., Richter, A., Schneider, M., Schrems, O., Silicani, M., Stiller, G. P., Taylor, J., Tétard, C., Toohy, M., Vanhellefont, F., Warneke, T., Zawodny, J. M., and Zou, J.: Validation of NO₂ and NO from the Atmospheric Chemistry Experiment (ACE), *Atmos. Chem. Phys.*, 8, 5801–5841, doi:10.5194/acp-8-5801-2008, 2008. 12742

LISIRD Data Systems Group: LISIRD: LASP Interactive Solar Irradiance Data Center, available at: <http://lasp.colorado.edu/lisird/> (last access: 30 September 2013), 2010. 12752

Merino, F., Murtagh, D., Ridal, M., Eriksson, P., Baron, P., Ricaud, P., and de la Noe, J.: Studies for the Odin sub-millimetre radiometer: III. Performance simulations, *Can. J. Phys.*, 80, 357–373, doi:10.1139/P01-154, 2002. 12743

Murtagh, D., Frisk, U., Merino, F., Ridal, M., Jonsson, A., Stegman, J., Witt, G., Eriksson, P., Jimenez, C., Megie, G., de la Noe, J., Ricaud, P., Baron, P., Pardo, J., Hauchcorne, A., Llewellyn, E., Degenstein, D., Gattinger, R., Lloyd, N., Evans, W., McDade, I., Haley, C., Sioris, C., von Savigny, C., Solheim, B., McConnell, J., Strong, K., Richardson, E., Lepelmeier, G., Kyrola, E., Auvinen, H., and Oikarinen, L.: An overview of the Odin atmospheric mission, *Can. J. Phys.*, 80, 309–319, doi:10.1139/P01-157, 2002. 12742

Neter, J., Kutner, M., Wasserman, W., and Nachtsheim, C.: *Applied Linear Statistical Models*, McGraw-Hill/Irwin, available at: <http://www.amazon.com/Applied-Linear-Statistical-Models->

NO MLT comparison of ACE-FTS, MIPAS, SCIAMACHY, and SMR

S. Bender et al.

Title Page

Abstract

Introduction

Conclusions

References

Tables

Figures



Back

Close

Full Screen / Esc

Printer-friendly Version

Interactive Discussion



Neter/dp/0256117365%3FSubscriptionId%3D0JYN1NVW651KCA56C102%26tag%3Dtechie-20%26linkCode%3Dxm2%26camp%3D2025%26creative%3D165953%26creativeASIN%3D0256117365 (last access: 7 October 2014), 1996. 12753

5 NGDC and NOAA: Space Physics Interactive Data Resource (SPIDR), available at: <http://spidr.ngdc.noaa.gov/spidr/> (last access: 11 December 2013), 2011. 12752

Nordh, H. L., von Schéele, F., Frisk, U., Ahola, K., Booth, R. S., Encrenaz, P. J., Hjalmarsen, Å., Kendall, D., Kyrölä, E., Kwok, S., Lecacheux, A., Leppelmeier, G., Llewellyn, E. J., Mattila, K., Mégie, G., Murtagh, D., Rougeron, M., and Witt, G.: The Odin orbital observatory, *Astron. Astrophys.*, 402, L21–L25, doi:10.1051/0004-6361:20030334, 2003. 12742

10 Pérot, K., Urban, J., and Murtagh, D. P.: Unusually strong nitric oxide descent in the Arctic middle atmosphere in early 2013 as observed by Odin/SMR, *Atmos. Chem. Phys.*, 14, 8009–8015, doi:10.5194/acp-14-8009-2014, 2014. 12743

Raspollini, P., Carli, B., Carlotti, M., Ceccherini, S., Dehn, A., Dinelli, B. M., Dudhia, A., Flaud, J.-M., López-Puertas, M., Niro, F., Remedios, J. J., Ridolfi, M., Sembhi, H., Sgheri, L., and von Clarman, T.: Ten years of MIPAS measurements with ESA Level 2 processor V6 – Part 1: Retrieval algorithm and diagnostics of the products, *Atmos. Meas. Tech.*, 6, 2419–2439, doi:10.5194/amt-6-2419-2013, 2013. 12739

15 Sheese, P. E., Strong, K., Gattinger, R. L., Llewellyn, E. J., Urban, J., Boone, C. D., and Smith, A. K.: Odin observations of Antarctic nighttime NO densities in the mesosphere-lower thermosphere and observations of a lower NO layer, *J. Geophys. Res.*, 118, 7414–7425, doi:10.1002/jgrd.50563, 2013. 12743

20 Urban, J., Lautie, N., Murtagh, D., Eriksson, P., Kasai, Y., Lossow, S., Dupuy, E., de la Noe, J., Frisk, U., Olberg, M., Le Flochmoen, E., and Ricaud, P.: Global observations of middle atmospheric water vapour by the Odin satellite: an overview, *Planet. Space Sci.*, 55, 1093–1102, doi:10.1016/j.pss.2006.11.021, 2007. 12743

25 von Clarman, T., Glatthor, N., Grabowski, U., Höpfner, M., Kellmann, S., Kiefer, M., Linden, A., Tsidu, G. M., Milz, M., Steck, T., Stiller, G. P., Wang, D. Y., Fischer, H., Funke, B., Gil-López, S., and López-Puertas, M.: Retrieval of temperature and tangent altitude pointing from limb emission spectra recorded from space by the Michelson Interferometer for Passive Atmospheric Sounding (MIPAS), *J. Geophys. Res.*, 108, 4736, doi:10.1029/2003JD003602, 2003. 12739

30

Waymark, C., Walker, K. A., Boone, C. D., and Bernath, P. F.: ACE-FTS version 3.0 data set: validation and data processing update, Ann. Geophys.-Italy, 56, doi:10.4401/ag-6339, Fast Track 1, 2013. 12742

AMTD

7, 12735–12794, 2014

NO MLT comparison of ACE-FTS, MIPAS, SCIAMACHY, and SMR

S. Bender et al.

Title Page

Abstract

Introduction

Conclusions

References

Tables

Figures



Back

Close

Full Screen / Esc

Printer-friendly Version

Interactive Discussion



NO MLT comparison of ACE-FTS, MIPAS, SCIAMACHY, and SMR

S. Bender et al.

Table 1. Instrument overview.

	SCISAT ACE-FTS	Odin SMR	MIPAS	Envisat SCIAMACHY
orbit		sun-synchronous		sun-synchronous
altitude	650 km	580 km		790 km
equatorial crossing time	variable	06:00–07:00/18:00–19:00		10:00/22:00
measurement type	solar occultation	limb	limb	limb
NO wavelength	infrared	sub-mm	infrared	ultra-violet
MLT measurement days	1941	301	199	78
MLT time period	2004–2010	2003–present	2005–2012	2008–2012
data version	3.0	2.1	V40 (2005–2009) V5R (2010–2012)	2.0

Title Page

Abstract

Introduction

Conclusions

References

Tables

Figures



Back

Close

Full Screen / Esc

Printer-friendly Version

Interactive Discussion



**NO MLT comparison
of ACE-FTS, MIPAS,
SCIAMACHY, and
SMR**

S. Bender et al.

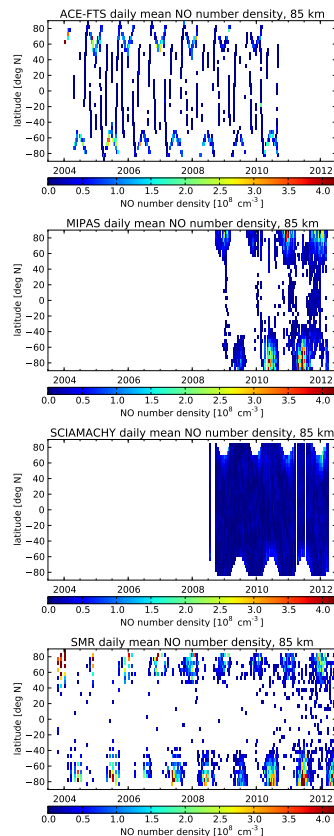


Figure 1. NO zonal mean time series at 85 km, ACE-FTS, MIPAS, SCIAMACHY, and SMR (from top to bottom).

Title Page

Abstract

Introduction

Conclusions

References

Tables

Figures



Back

Close

Full Screen / Esc

Printer-friendly Version

Interactive Discussion



**NO MLT comparison
of ACE-FTS, MIPAS,
SCIAMACHY, and
SMR**

S. Bender et al.

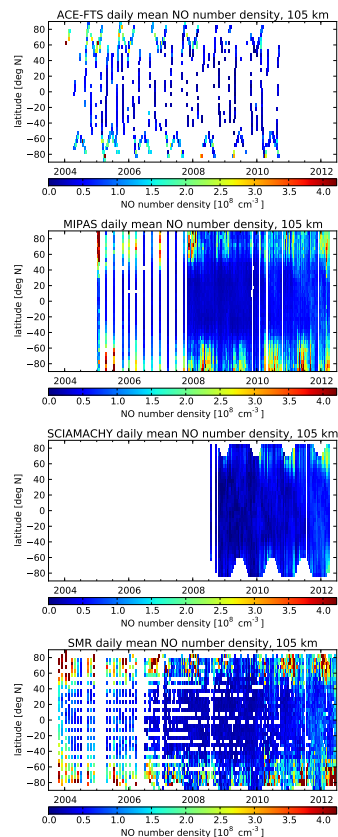


Figure 2. NO zonal mean time series at 105 km, ACE-FTS, MIPAS, SCIAMACHY, and SMR (from top to bottom).

Title Page

Abstract

Introduction

Conclusions

References

Tables

Figures



Back

Close

Full Screen / Esc

Printer-friendly Version

Interactive Discussion



**NO MLT comparison
of ACE-FTS, MIPAS,
SCIAMACHY, and
SMR**

S. Bender et al.

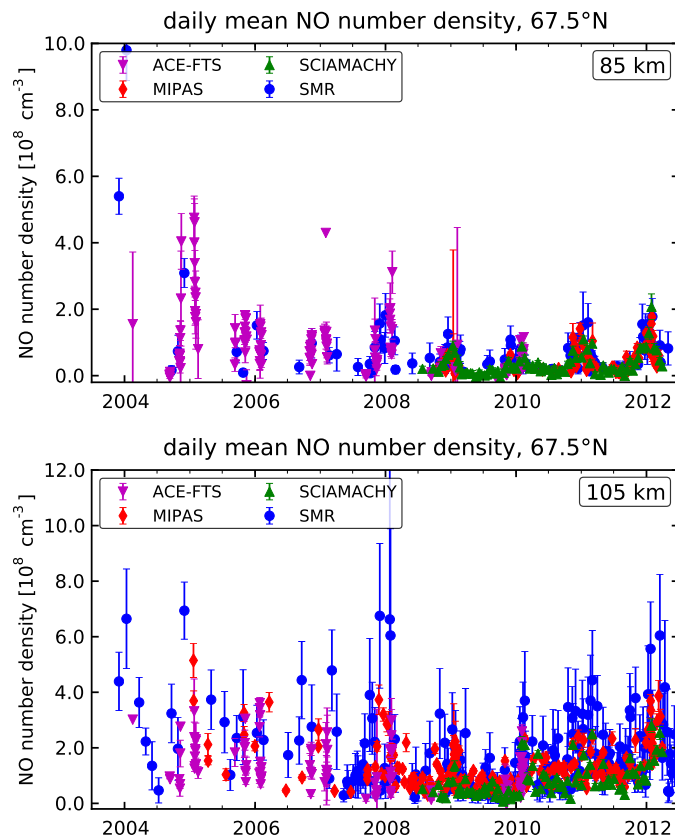
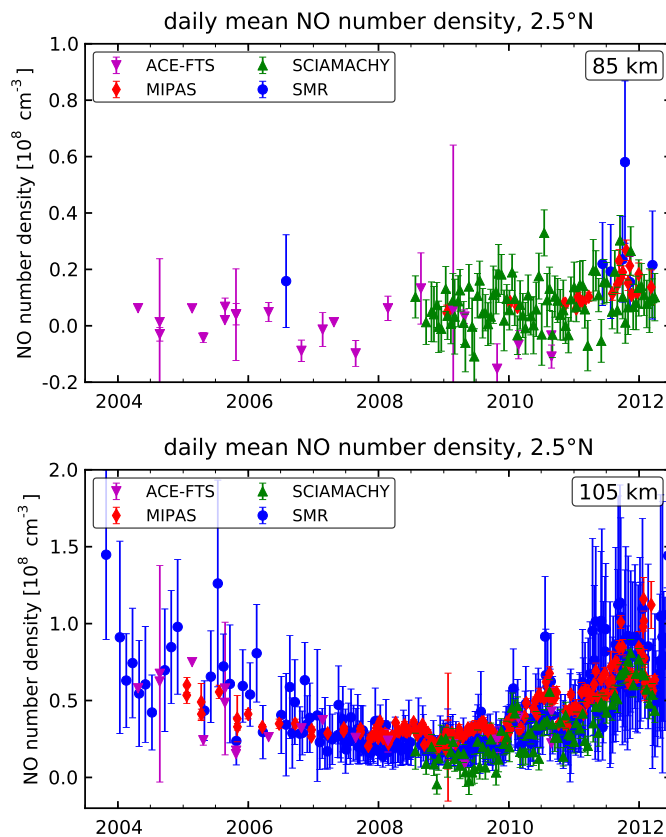


Figure 3. NO time series comparison of all four instruments at 67.5° N, for 85 km (top) and 105 km (bottom). The error bars indicate the 95 % confidence interval of the daily zonal mean.

**NO MLT comparison
of ACE-FTS, MIPAS,
SCIAMACHY, and
SMR**

S. Bender et al.

**Figure 6.** NO time series comparison as in Fig. 3 for 2.5° N.

NO MLT comparison of ACE-FTS, MIPAS, SCIAMACHY, and SMR

S. Bender et al.

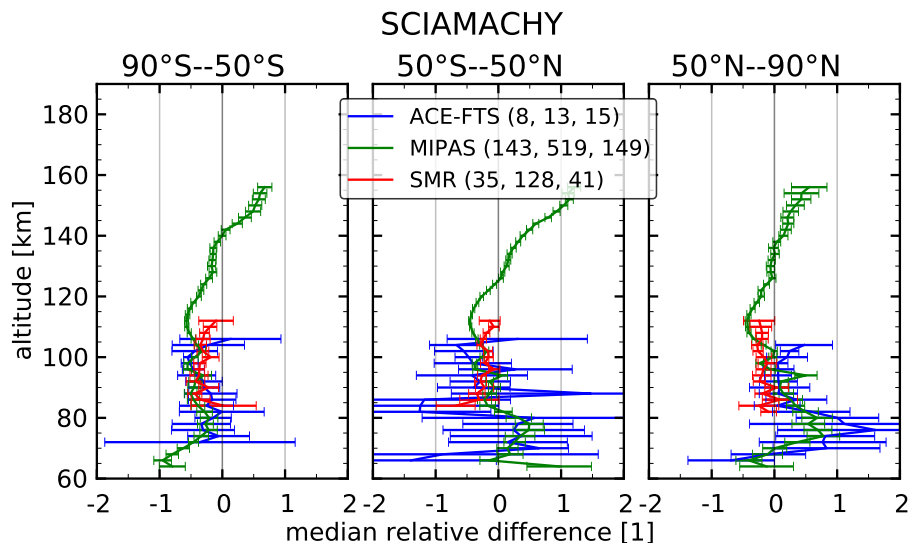


Figure 7. NO vertical profile comparison of the SCIAMACHY NO number density ($n_{\text{NO}}^{\text{SCIAMACHY}}$) to the other instruments ($n_{\text{NO}}^{\text{other}}$). Shown is the median of the relative differences ($n_{\text{NO}}^{\text{SCIAMACHY}} - n_{\text{NO}}^{\text{other}}/n_{\text{NO}}^{\text{other}}$) averaged over days coincident with other observations. The panels show the results in the southern polar region (left), at middle and low latitudes (middle), and in the northern polar region (right). The error bars indicate the 95 % confidence interval using the median absolute deviation ($3 \times \text{MAD}$). The numbers in parentheses denote the number of coincident profiles in these three regions from south (left) to north (right).

Title Page

Abstract

Introduction

Conclusions

References

Tables

Figures

◀

▶

◀

▶

Back

Close

Full Screen / Esc

Printer-friendly Version

Interactive Discussion



NO MLT comparison of ACE-FTS, MIPAS, SCIAMACHY, and SMR

S. Bender et al.

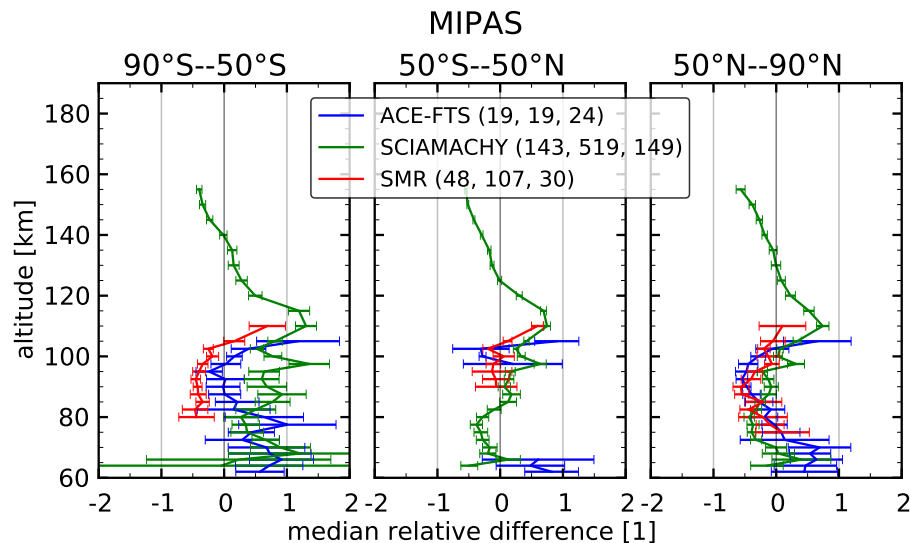


Figure 8. NO vertical profile comparison of MIPAS NO data $n_{\text{NO}}^{\text{MIPAS}}$. For a detailed description see Fig. 7.

Title Page

Abstract

Introduction

Conclusions

References

Tables

Figures

◀

▶

◀

▶

Back

Close

Full Screen / Esc

Printer-friendly Version

Interactive Discussion



**NO MLT comparison
of ACE-FTS, MIPAS,
SCIAMACHY, and
SMR**

S. Bender et al.

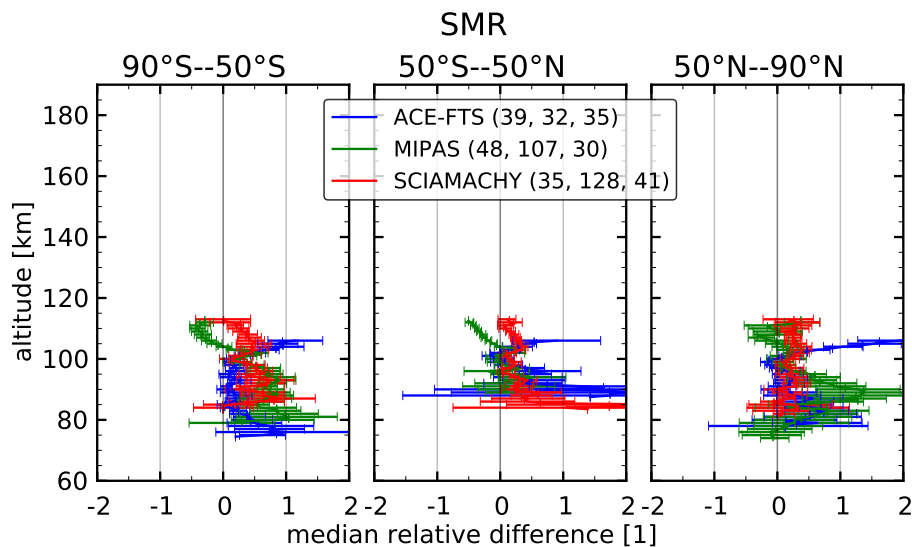


Figure 9. NO vertical profile comparison of the SMR data $n_{\text{NO}}^{\text{SMR}}$. See Fig. 7 for details.

[Title Page](#)[Abstract](#)[Introduction](#)[Conclusions](#)[References](#)[Tables](#)[Figures](#)[◀](#)[▶](#)[◀](#)[▶](#)[Back](#)[Close](#)[Full Screen / Esc](#)[Printer-friendly Version](#)[Interactive Discussion](#)

NO MLT comparison of ACE-FTS, MIPAS, SCIAMACHY, and SMR

S. Bender et al.

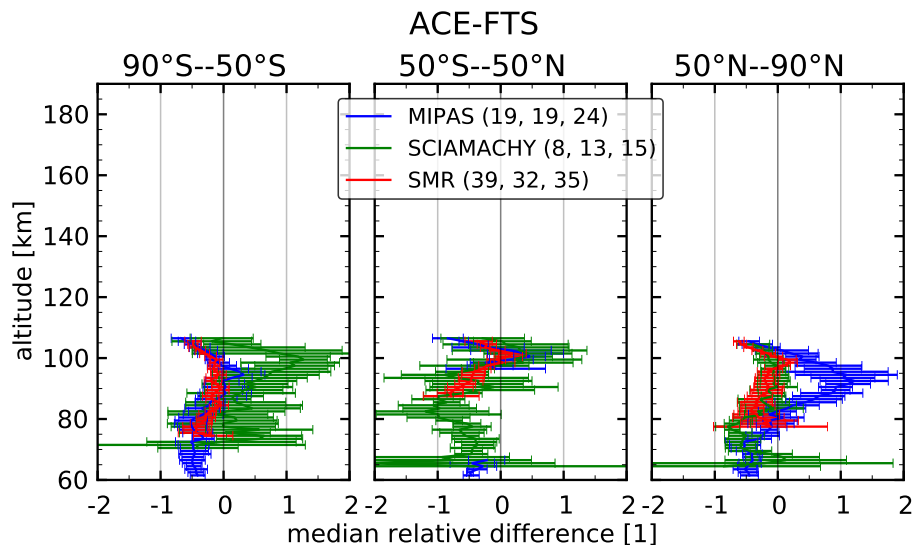


Figure 10. NO vertical profile comparison of the ACE-FTS data $n_{\text{NO}}^{\text{ACE-FTS}}$. See Fig. 7 for details.

Title Page

Abstract

Introduction

Conclusions

References

Tables

Figures

◀

▶

◀

▶

Back

Close

Full Screen / Esc

Printer-friendly Version

Interactive Discussion



NO MLT comparison of ACE-FTS, MIPAS, SCIAMACHY, and SMR

S. Bender et al.

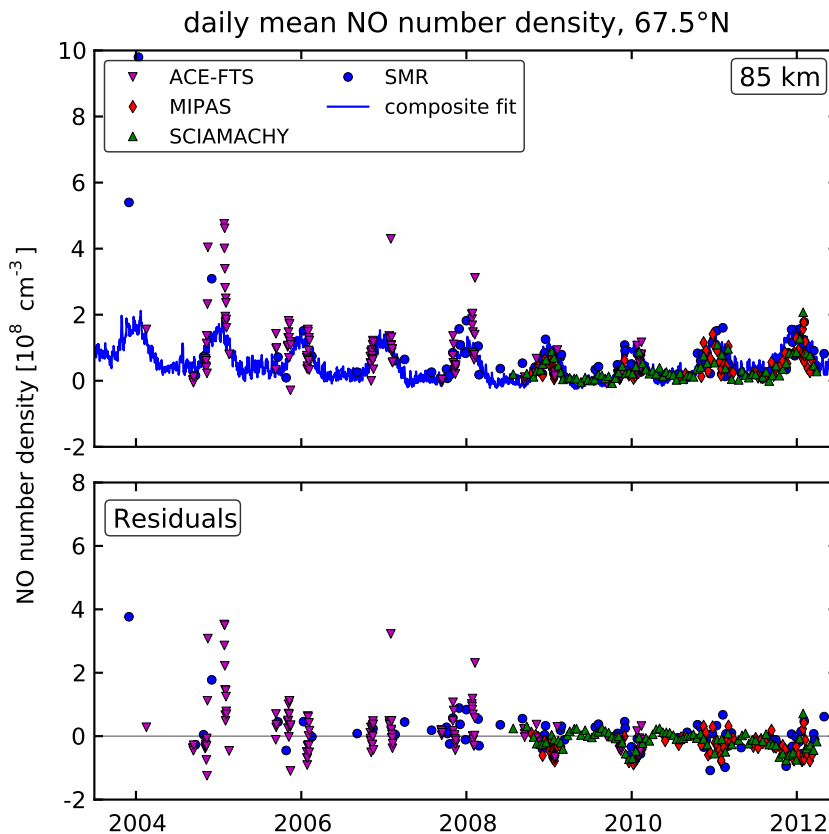


Figure 11. NO time series regression results at 67.5° N, 85 km. The upper panel shows the individual time series and the composite regression fit using all data simultaneously. The lower panel shows the residuals.

Title Page

Abstract

Introduction

Conclusions

References

Tables

Figures

◀

▶

◀

▶

Back

Close

Full Screen / Esc

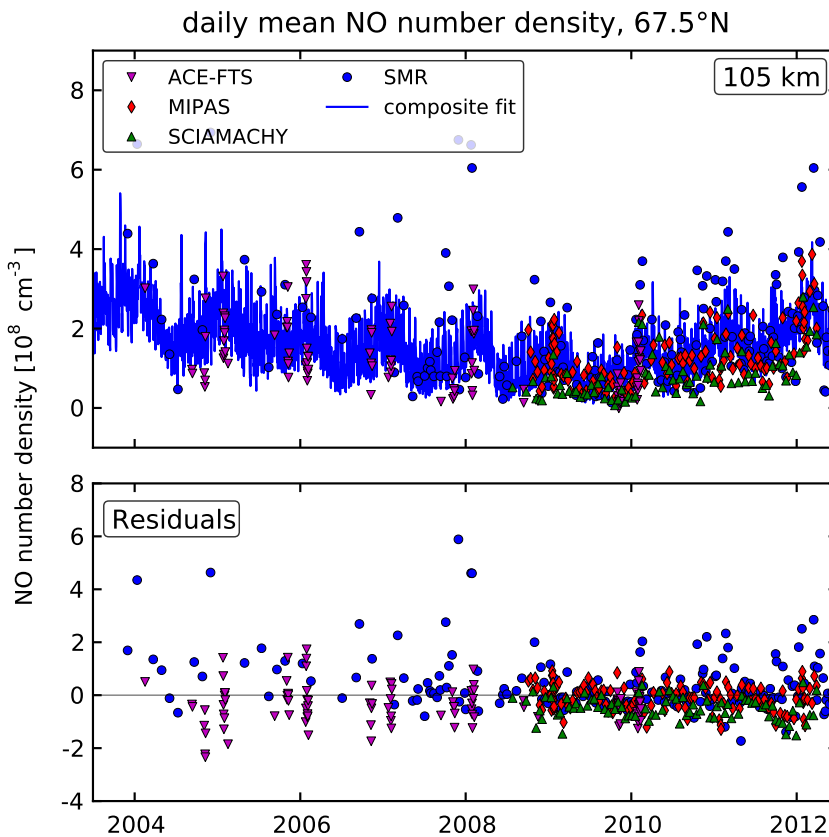
Printer-friendly Version

Interactive Discussion



**NO MLT comparison
of ACE-FTS, MIPAS,
SCIAMACHY, and
SMR**

S. Bender et al.

**Figure 12.** NO time series regression results at 67.5° N, 105 km as in Fig. 11.

Title Page

Abstract

Introduction

Conclusions

References

Tables

Figures

◀

▶

◀

▶

Back

Close

Full Screen / Esc

Printer-friendly Version

Interactive Discussion



NO MLT comparison of ACE-FTS, MIPAS, SCIAMACHY, and SMR

S. Bender et al.

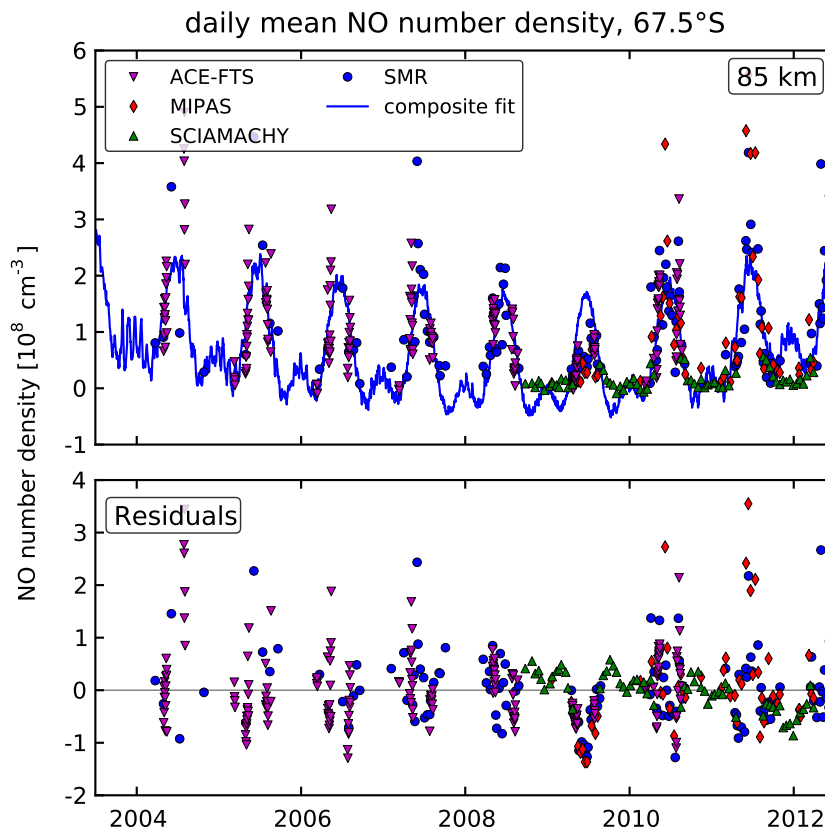


Figure 13. NO time series regression results at 67.5° S, 85 km as in Fig. 11.

Title Page	
Abstract	Introduction
Conclusions	References
Tables	Figures
◀	▶
◀	▶
Back	Close
Full Screen / Esc	
Printer-friendly Version	
Interactive Discussion	



NO MLT comparison of ACE-FTS, MIPAS, SCIAMACHY, and SMR

S. Bender et al.

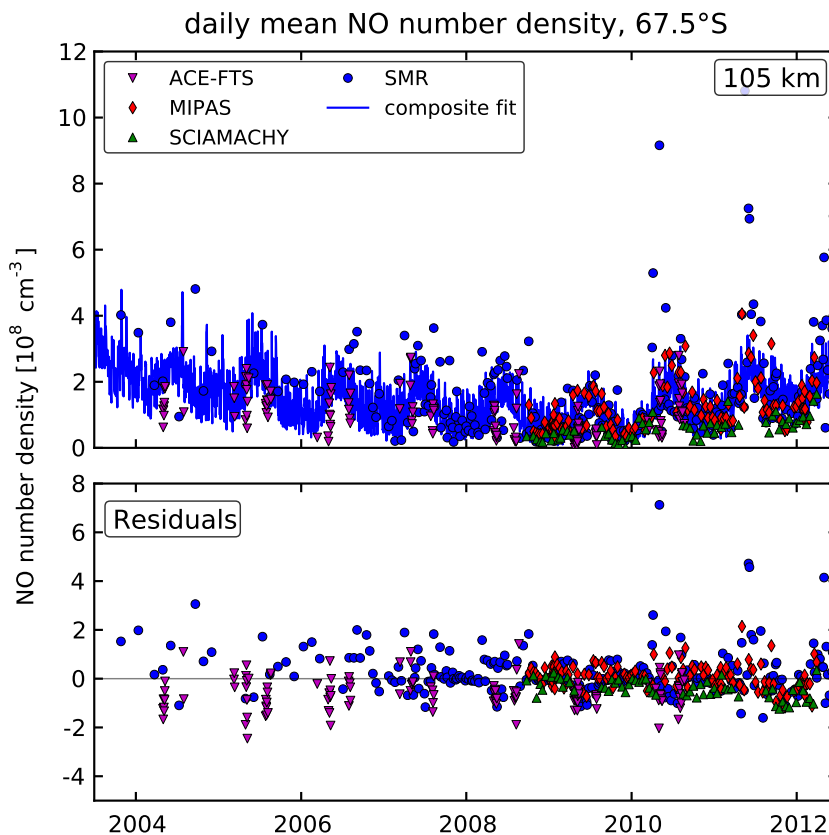


Figure 14. NO time series regression results at 67.5° S, 105 km as in Fig. 11.

Title Page	
Abstract	Introduction
Conclusions	References
Tables	Figures
◀	▶
◀	▶
Back	Close
Full Screen / Esc	
Printer-friendly Version	
Interactive Discussion	



**NO MLT comparison
of ACE-FTS, MIPAS,
SCIAMACHY, and
SMR**

S. Bender et al.

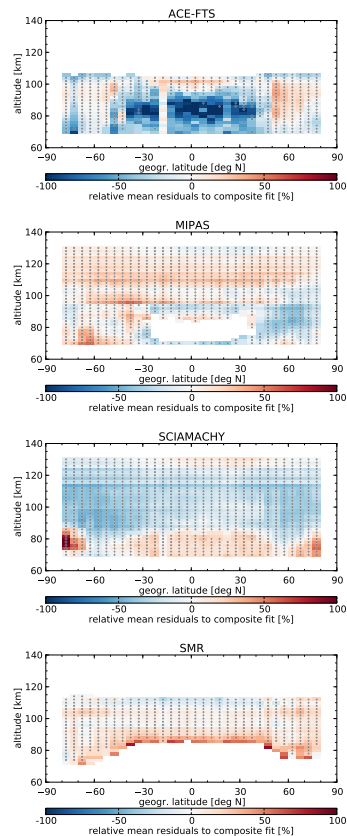


Figure 15. NO mean residuals of the individual measurements to the composite fit. The marked boxes indicate a larger than 95 % significance determined using the F test of the regression fit.

[Title Page](#)[Abstract](#)[Introduction](#)[Conclusions](#)[References](#)[Tables](#)[Figures](#)[◀](#)[▶](#)[◀](#)[▶](#)[Back](#)[Close](#)[Full Screen / Esc](#)[Printer-friendly Version](#)[Interactive Discussion](#)

NO MLT comparison of ACE-FTS, MIPAS, SCIAMACHY, and SMR

S. Bender et al.

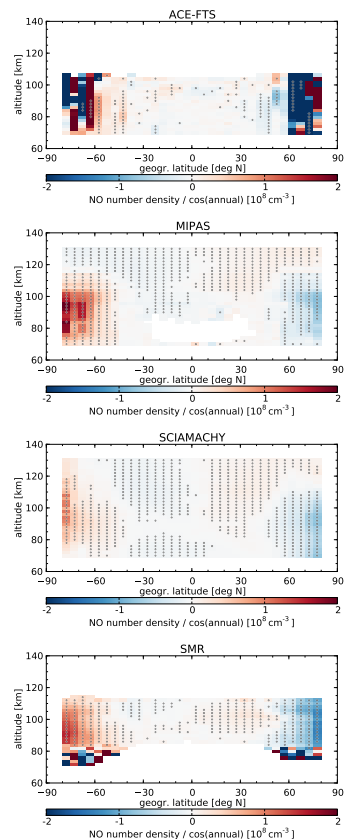


Figure 16. NO regression coefficient d_1 of the annual cycle (cosine part). The marked boxes indicate a larger than 95 % significance of the coefficient calculated using the t test.

Title Page

Abstract

Introduction

Conclusions

References

Tables

Figures

◀

▶

◀

▶

Back

Close

Full Screen / Esc

Printer-friendly Version

Interactive Discussion



NO MLT comparison of ACE-FTS, MIPAS, SCIAMACHY, and SMR

S. Bender et al.

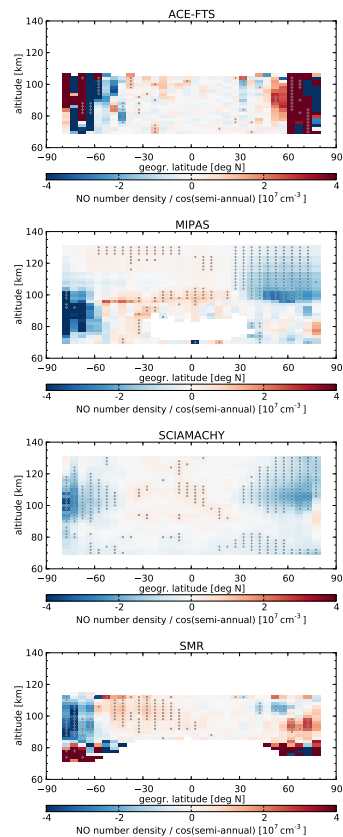


Figure 17. NO regression coefficient d_2 of the semi-annual cycle (cosine part) as in Fig. 16.

Title Page

Abstract

Introduction

Conclusions

References

Tables

Figures

◀

▶

◀

▶

Back

Close

Full Screen / Esc

Printer-friendly Version

Interactive Discussion



NO MLT comparison of ACE-FTS, MIPAS, SCIAMACHY, and SMR

S. Bender et al.

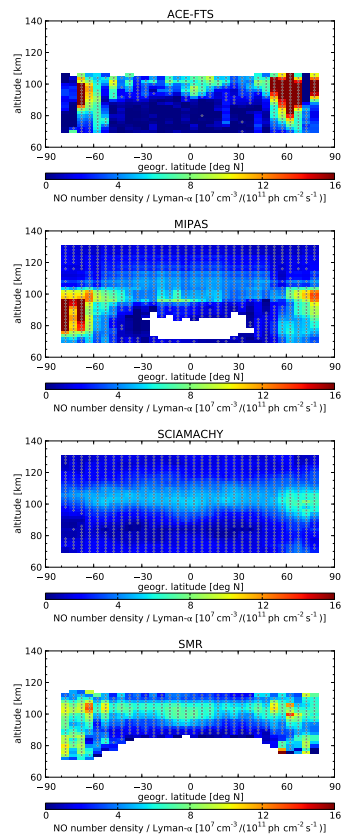


Figure 18. NO regression coefficient b of the long-term solar UV variations from the Lyman- α index as in Fig. 16.

[Title Page](#)
[Abstract](#)
[Introduction](#)
[Conclusions](#)
[References](#)
[Tables](#)
[Figures](#)
[Back](#)
[Close](#)
[Full Screen / Esc](#)
[Printer-friendly Version](#)
[Interactive Discussion](#)

NO MLT comparison of ACE-FTS, MIPAS, SCIAMACHY, and SMR

S. Bender et al.

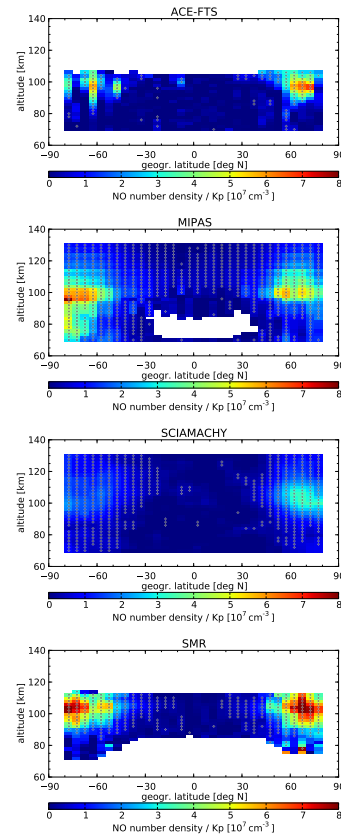


Figure 19. NO regression coefficient c of the short-term geomagnetic variations from the Kp index as in Fig. 16.

[Title Page](#)
[Abstract](#)
[Introduction](#)
[Conclusions](#)
[References](#)
[Tables](#)
[Figures](#)
[Back](#)
[Close](#)
[Full Screen / Esc](#)
[Printer-friendly Version](#)
[Interactive Discussion](#)


**NO MLT comparison
of ACE-FTS, MIPAS,
SCIAMACHY, and
SMR**

S. Bender et al.

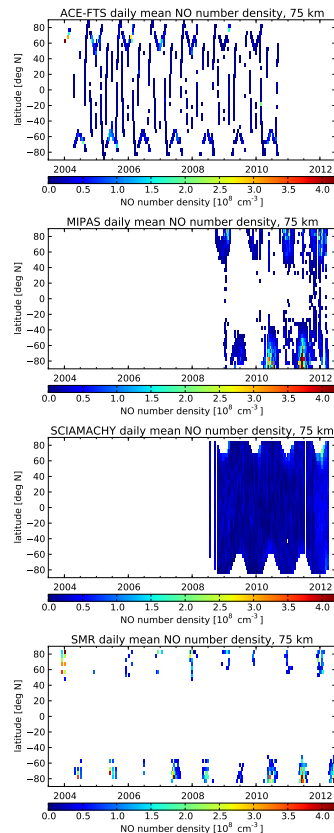


Figure A1. NO zonal mean time series at 75 km, ACE-FTS, MIPAS, SCIAMACHY, and SMR (from top to bottom).

Title Page

Abstract

Introduction

Conclusions

References

Tables

Figures

◀

▶

◀

▶

Back

Close

Full Screen / Esc

Printer-friendly Version

Interactive Discussion



**NO MLT comparison
of ACE-FTS, MIPAS,
SCIAMACHY, and
SMR**

S. Bender et al.

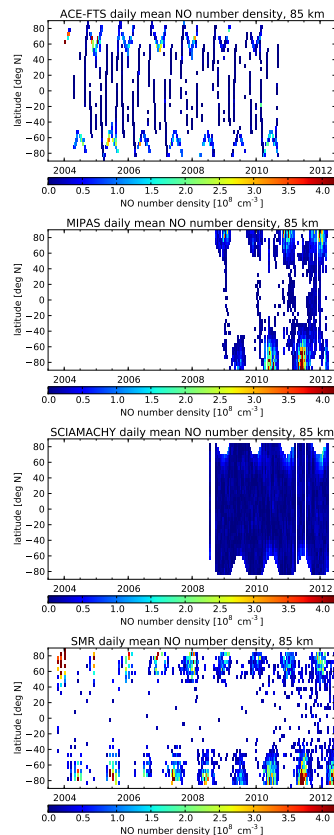


Figure A2. NO zonal mean time series at 85 km, ACE-FTS, MIPAS, SCIAMACHY, and SMR (from top to bottom).

[Title Page](#)[Abstract](#)[Introduction](#)[Conclusions](#)[References](#)[Tables](#)[Figures](#)[◀](#)[▶](#)[◀](#)[▶](#)[Back](#)[Close](#)[Full Screen / Esc](#)[Printer-friendly Version](#)[Interactive Discussion](#)

AMTD

7, 12735–12794, 2014

NO MLT comparison of ACE-FTS, MIPAS, SCIAMACHY, and SMR

S. Bender et al.

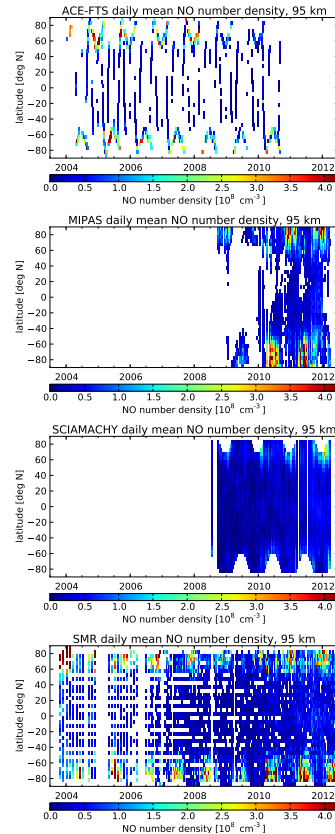


Figure A3. NO zonal mean time series at 95 km, ACE-FTS, MIPAS, SCIAMACHY, and SMR (from top to bottom).

Title Page

Abstract

Introduction

Conclusions

References

Tables

Figures

◀

▶

◀

▶

Back

Close

Full Screen / Esc

Printer-friendly Version

Interactive Discussion



**NO MLT comparison
of ACE-FTS, MIPAS,
SCIAMACHY, and
SMR**

S. Bender et al.

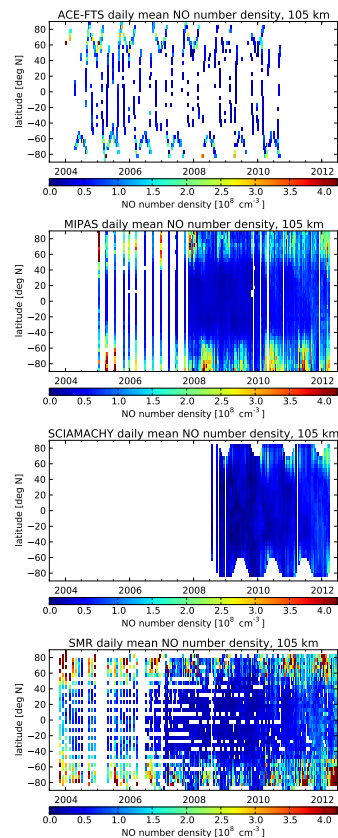


Figure A4. NO zonal mean time series at 105 km, ACE-FTS, MIPAS, SCIAMACHY, and SMR (from top to bottom).

Title Page

Abstract

Introduction

Conclusions

References

Tables

Figures

◀

▶

◀

▶

Back

Close

Full Screen / Esc

Printer-friendly Version

Interactive Discussion



**NO MLT comparison
of ACE-FTS, MIPAS,
SCIAMACHY, and
SMR**

S. Bender et al.

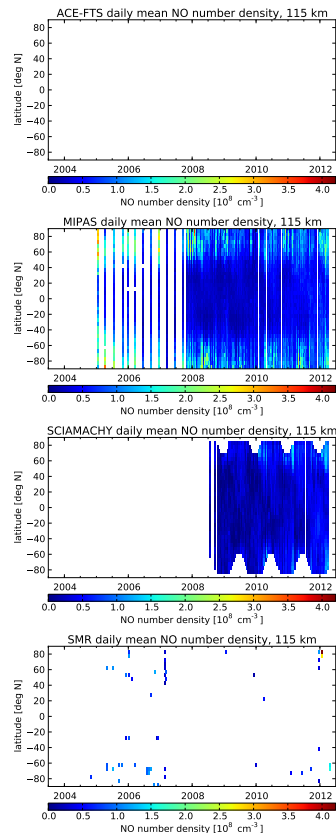


Figure A5. NO zonal mean time series at 115 km, ACE-FTS, MIPAS, SCIAMACHY, and SMR (from top to bottom).

Title Page

Abstract

Introduction

Conclusions

References

Tables

Figures

◀

▶

◀

▶

Back

Close

Full Screen / Esc

Printer-friendly Version

Interactive Discussion



**NO MLT comparison
of ACE-FTS, MIPAS,
SCIAMACHY, and
SMR**

S. Bender et al.

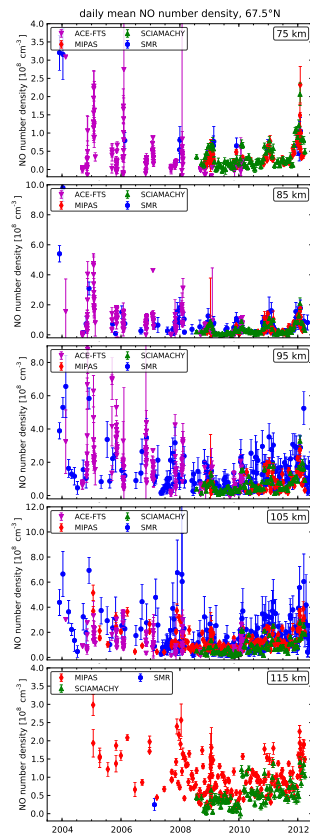


Figure B1. NO time series comparison of all four instruments at 67.5° N, for 75, 85, 95, 105, and 115 km (from top to bottom).

[Title Page](#)[Abstract](#)[Introduction](#)[Conclusions](#)[References](#)[Tables](#)[Figures](#)[◀](#)[▶](#)[◀](#)[▶](#)[Back](#)[Close](#)[Full Screen / Esc](#)[Printer-friendly Version](#)[Interactive Discussion](#)

**NO MLT comparison
of ACE-FTS, MIPAS,
SCIAMACHY, and
SMR**

S. Bender et al.

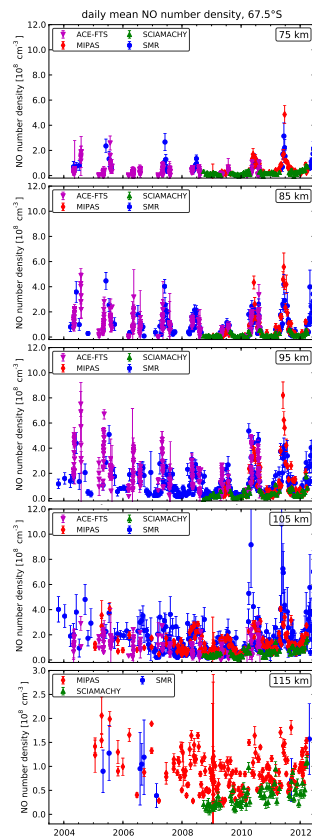


Figure B2. NO time series comparison of all four instruments at 67.5° S, for 75, 85, 95, 105, and 115 km (from top to bottom).

[Title Page](#)[Abstract](#)[Introduction](#)[Conclusions](#)[References](#)[Tables](#)[Figures](#)[◀](#)[▶](#)[◀](#)[▶](#)[Back](#)[Close](#)[Full Screen / Esc](#)[Printer-friendly Version](#)[Interactive Discussion](#)

**NO MLT comparison
of ACE-FTS, MIPAS,
SCIAMACHY, and
SMR**

S. Bender et al.

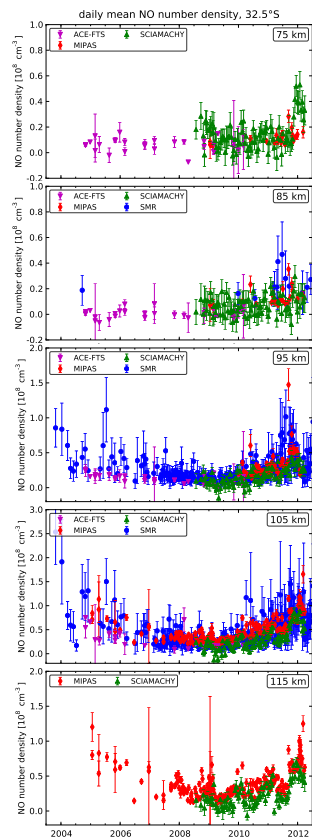


Figure B3. NO time series comparison of all four instruments at 32.5° S, for 75, 85, 95, 105, and 115 km (from top to bottom).

[Title Page](#)[Abstract](#)[Introduction](#)[Conclusions](#)[References](#)[Tables](#)[Figures](#)[Back](#)[Close](#)[Full Screen / Esc](#)[Printer-friendly Version](#)[Interactive Discussion](#)

**NO MLT comparison
of ACE-FTS, MIPAS,
SCIAMACHY, and
SMR**

S. Bender et al.

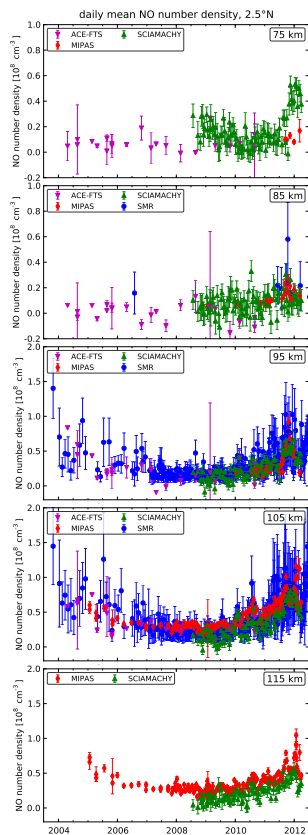


Figure B4. NO time series comparison of all four instruments at 2.5° N, for 75, 85, 95, 105, and 115 km (from top to bottom).

Title Page

Abstract

Introduction

Conclusions

References

Tables

Figures



Back

Close

Full Screen / Esc

Printer-friendly Version

Interactive Discussion



**NO MLT comparison
of ACE-FTS, MIPAS,
SCIAMACHY, and
SMR**

S. Bender et al.

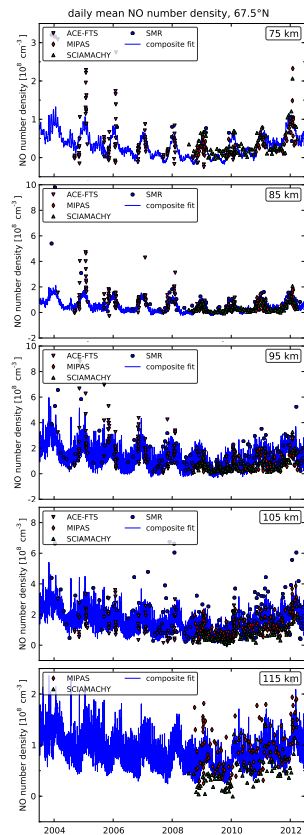


Figure C1. NO time series regression results at 67.5° N, for 75, 85, 95, 105, and 115 km (from top to bottom).

Title Page

Abstract

Introduction

Conclusions

References

Tables

Figures



Back

Close

Full Screen / Esc

Printer-friendly Version

Interactive Discussion



**NO MLT comparison
of ACE-FTS, MIPAS,
SCIAMACHY, and
SMR**

S. Bender et al.

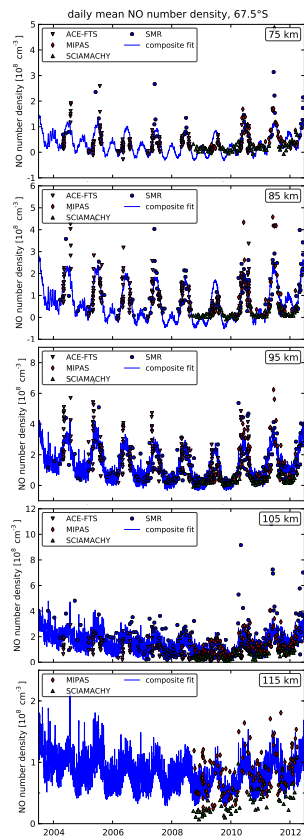


Figure C2. NO time series regression results at 67.5° S, for 75, 85, 95, 105, and 115 km (from top to bottom).

Title Page

Abstract

Introduction

Conclusions

References

Tables

Figures

◀

▶

◀

▶

Back

Close

Full Screen / Esc

Printer-friendly Version

Interactive Discussion



**NO MLT comparison
of ACE-FTS, MIPAS,
SCIAMACHY, and
SMR**

S. Bender et al.

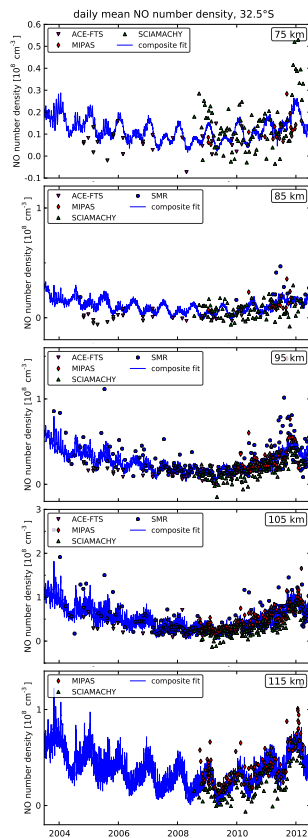


Figure C3. NO time series regression results at 32.5° S, for 75, 85, 95, 105, and 115 km (from top to bottom).

Title Page

Abstract

Introduction

Conclusions

References

Tables

Figures

◀

▶

◀

▶

Back

Close

Full Screen / Esc

Printer-friendly Version

Interactive Discussion



**NO MLT comparison
of ACE-FTS, MIPAS,
SCIAMACHY, and
SMR**

S. Bender et al.

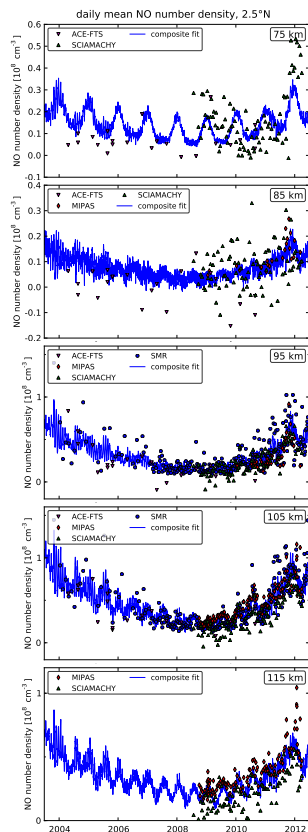


Figure C4. NO time series regression results at 2.5° N, for 75, 85, 95, 105, and 115 km (from top to bottom).

Title Page

Abstract

Introduction

Conclusions

References

Tables

Figures

◀

▶

◀

▶

Back

Close

Full Screen / Esc

Printer-friendly Version

Interactive Discussion

